Characterizing the origins of dissolved organic carbon in coastal seawater using stable carbon isotope and light absorption characteristics

Heejun Han[1], Jeomshik Hwang[1], Guebuem Kim[1]

[1]School of Earth and Environmental Sciences/Research Institute of Oceanography, Seoul National University, Seoul, 08826, South Korea

Correspondence to: Guebuem Kim (gkim@snu.ac.kr)

Abstract. In order to determine the origins of dissolved organic matter (DOM) occurring in the coastal seawater of Sihwa Lake, a water body semi-enclosed by a dyke along the western coast of South Korea, we measured the stable carbon isotope ratios of dissolved organic carbon (DOC–δ^{13}C) and the optical properties (absorbance and fluorescence) of DOM in two different seasons (March 2017 and September 2018). The concentrations of DOC were generally higher in lower salinity waters in both periods, and excess of DOC was also observed in 2017 in high-salinity waters. The higher concentrations of DOC in the lower salinity waters originated mainly from marine sediments of tidal flats, based on the DOC–δ^{13}C values (–20.7±1.2‰) and good correlations among the DOC, humic-like fluorescent DOM (FDOM$_H$), and NH$_4^+$ concentrations. However, the origins of the excess DOC observed in 2017 appears to be from two different sources: one mainly from marine sources such as biological production based on the DOC–δ^{13}C values (–19.1‰ to –20.5‰), and the other mainly from terrestrial sources by land-seawater interactions based on its depleted DOC–δ^{13}C values (–21.5‰ to –27.8‰). This land-derived DOM observed in 2017 was likely associated with DOM on the reclaimed land, which experienced extended exposure to light and bacterial degradation as indicated by the higher spectral slope ratio (S_R) of light absorbance and no concurrent increases in the FDOM$_H$ and NH$_4^+$ concentrations. Our study demonstrates that the combination of these biogeochemical tools can be a powerful tracer of DOM sources in coastal environments.

1 Introduction

Dissolved organic carbon (DOC), a major component of dissolved organic matter (DOM), is the largest reduced carbon pool in the ocean (Benner et al., 1992; Raymond and Spencer, 2014). DOC plays a significant role in coastal carbon dynamics and biogeochemical cycles and thus it is important to understand the sources and characteristics of DOC (Vetter et al., 2007; Carson and Hansell, 2015). In the coastal ocean, DOM sources include (1) in-situ biological production (Carlson and Hansell, 2015), (2) terrestrial organic matter such as soils and plant matters (Opsahl and Benner, 1997; Bauer and Bianchi, 2011), and (3) anthropogenic sources such as industrial and agricultural wastewaters (Tedetti et al., 2010; Griffith and Raymond, 2011).

A part of DOM is known as colored dissolved organic matter (CDOM), which is the light-absorbing fraction of organic matter (Coble, 2007; Kim and Kim, 2016; Kim and Kim, 2018). The major fraction of CDOM, which emits fluorescence after absorbing light energy, is referred to as fluorescent DOM (FDOM) (Coble, 1996; Coble, 2007; Kim and Kim, 2016). Rivers are known as the major source of the humic-like FDOM ($FDOM_H$) in the coastal ocean (Stedmon and Nelson, 2015; Kim and Kim, 2016), while aerobic microbial remineralization of sinking organic matter is the major source of $FDOM_H$ in the deep sea (Jørgensen et al., 2011; Catalá et al., 2015; Kim and Kim, 2016). On the other hand, Kim and Kim (2016) reported that anaerobic production in the bottom sediment of the deep East Sea (Japan Sea) accounted for approximately 10% of the total production of $FDOM_H$ in a deep water column. Recently, the anaerobic process in the bottom sediment of coastal oceans was suggested as an important source of $FDOM_H$ (Kim and Kim, 2018).

In order to decipher the sources of $FDOM_H$ and DOC in coastal waters, various approaches including optical properties and stable carbon isotope ratios ($\delta^{13}C$) have been developed. The humic-like component and protein-like component of FDOM were identified based on an excitation-emission matrix (EEM) spectroscopy method combined with a parallel factor analysis (PARAFAC) model (Bro, 1997; Coble, 2007; Kim and Kim, 2016; Kim and Kim 2018). The molecular weight and photochemical processes of DOM were characterized by the absorption spectra and spectral parameters of CDOM. For example, the absorption spectral slope ratio (S_R) negatively correlates with the DOM molecular weight and increases upon irradiation (Helms et al., 2008; Hansen et al., 2016). The stable carbon isotopic composition of DOC (DOC–$\delta^{13}C$) has been used to differentiate terrestrial versus marine DOC (Gearing, 1988; Wang et al., 2004; Lee and Kim, 2018; Lee et al., 2020). In general, $\delta^{13}C$ values of terrestrial sources such as C_3 and C_4 plants range from –23‰ to –34‰ and –9‰ to –17‰, respectively, while those derived from marine phytoplankton were found to range from –18‰ to –22‰ (Gearing, 1998).

In this study, we used DOC–$\delta^{13}C$, FDOM, and S_R values together to characterize different sources of DOM in Sihwa Lake, South Korea, one of the most dynamic coastal settings in terms of salinity changes, hypoxia, metal pollution, and eutrophication (Kim et al., 2009; Ra et al., 2011; Lee et al., 2014; Kim and Kim, 2014; Lee et al., 2017; Kim and Kim, 2018).

2 Materials and methods

2.1 Study area and sampling

Sihwa Lake (126.6 °E; 37.3 °N) is located on the western coast of South Korea, with an area of 57 km^2 and average depth of 3.2 m (maximum depth: 18 m). This lake was originally constructed as a land reclamation project planned by the government to provide agricultural land and water for the nearby metropolitan area during the 1980s and 1990s (Bae et al.,

2010) (Fig. 1). Freshwater runs through six small streams into the lake, and four waterways connect the lake to the Banwol industrial complex (Fig. 1). Because the lake experienced serious deterioration of its water quality owing to wastewater discharges from industrial complexes under limited water circulation, sluice gates were constructed and opened twice a day for water exchanges between the lake and the Yellow Sea since 2012. The dyke is currently used as a tidal power plant (Lee et al., 2017) (Fig. 1). The total volume of Sihwa Lake water is ~3.3×10^8 m^3. The water exchange rate is approximately 3.4×10^8 m^3 y^{-1}, enough to replace the entire reservoir in a year (Lee et al., 2003; Lee et al., 2014).

Water samples for the entire water column were collected on board a ship (~1 ton) in March 2017 and September 2018. In 2018, only surface water samples were collected at shallow stations (station numbers 1–6) as the water level of the reservoir was lower than in 2017. In order to investigate the effect of wastewater from the industrial complex, an additional sample was collected near the Banwol waterway (station B4) in 2018 (Fig. 1). The temperature and salinity were measured using a conductivity-temperature-depth (CTD) instrument (Ocean Seven 304, INDONAUT Srl).

The water samples were filtered through a pre-combusted (450 °C for 5h) GF/F filter (pore size: 0.7 μm; Whatman). The samples for the DOC and DOC–δ^{13}C analyses were acidified with 6M HCl (to a final sample pH of ~2) to avoid any bacterial activity and were stored in pre-combusted glass ampoules (Kim and Kim, 2010). Samples for the FDOM analysis were stored in pre-combusted amber vials in a refrigerator at 4°C. Samples for the dissolved inorganic nutrient analysis were stored frozen in polypropylene conical tubes.

2.2 Chemical analyses

Inorganic nutrient concentrations were measured using a nutrient auto-analyzer (New QuAAtro39, SEAL analytical). The analytical uncertainties were <5% for the reference materials for NO$_X$ (KANSO Co., LTD). The dissolved oxygen (DO) concentration was determined using Winkler's method (Carpenter, 1965). The DOC concentration was measured using a high-temperature catalytic oxidation (HTCO) method using a total organic carbon (TOC) analyzer (TOC-V$_{CPH}$, Shimadzu) (Kim and Kim, 2010). The accuracy of the DOC measurements was ±2 μmol L^{-1} for a certified reference material of deep seawater (DSR; ~43 μmol L^{-1} DOC; University of Miami) (Hansell, 2005). The DOC–δ^{13}C values were measured using an isotope ratio mass spectrometer (IRMS; Isoprime, Elementar) connected to a TOC analyzer (Vario TOC cube, Elementar) (Panetta et al., 2008; Troyer et al., 2010). The DOC–δ^{13}C values were in very good agreement, within <5%, with the reported values of the reference materials: IAEA-CH6 sucrose (δ^{13}C = −10.45±0.03‰), Suwannee River Fulvic Acid (SRFA; δ^{13}C = −27.6±0.12‰; International Humic Substances Society), and DSR (University of Miami) as reported by Lang et al. (2007) (δ^{13}C = −21.7±0.3‰) and Panetta et al. (2008) (δ^{13}C = −21.4±0.3‰).

2.3 Optical measurements

Fluorescence and absorbance spectra of the samples were measured using a spectrophotometer (Aqualog, Horiba). For the FDOM analysis, the emission and excitation wavelength ranges were set from 240 to 600 nm and from 250 to 500 nm, respectively, with 3 nm scanning intervals. The PARAFAC analysis for the EEM data was conducted using the Solo software (Eigenvector, 108 Inc.) (Han et al., 2020). The Raman and Rayleigh scattering signals, inner-filter effect, and blank subtraction were corrected with Milli-Q water (18.2 MΩcm) using the Solo software (Bro, 1997; Zepp et al., 2004; Stedmon and Bro, 2008; Han et al., 2020). The PARAFAC results were validated by a split-half analysis and random initialization (Stedmon and Bro, 2008). The fluorescence intensities of FDOM were normalized with the Raman peak area of water and were presented in Raman Unit (RU) (Lawaetz and Stedmon, 2009).

The PARAFAC model characterized one marine humic-like, one protein-like, and two terrestrial humic-like fluorescent components in Sihwa Lake, which are consistent with those of a previous study (Kim and Kim, 2018) (Fig. S1). The spectral shapes of the fluorescent components were compared with those in other results in the OpenFluor database (https://openfluor.lablicate.com) (Murphy et al., 2014). All components (C1 to C4) were matched with the major components from 36, 39, 62, and 19 studies, respectively, with similarity scores of 95%. The spectral characteristics of component 1 ($FDOM_C$; Ex/Em = 342/427 nm) and component 3 ($FDOM_A$; Ex/Em = 381/493 nm) are known to be associated with terrestrial humic-like DOM (Coble 2007). Component 2 ($FDOM_M$; Ex/Em = 297/388 nm) is known to be associated with marine humic-like DOM originating from microbial remineralization (Coble, 2007; Jørgensen et al., 2011). Component 4 ($FDOM_P$; Ex/Em = 282/322 nm) is characterized as a protein-like (tryptophan-like) DOM, which originates mainly from biological production (Coble, 2007). In this study, $FDOM_C$ was used as a representative of humic FDOM ($FDOM_H$) since all humic-like components showed similar patterns.

UV-visible absorption spectra of the samples were measured with a scanning wavelength range of 240–700 nm. The absorption coefficient was calculated using the following equation:

$$a_\lambda = 2.303 A_\lambda / l \tag{1}$$

where α is the absorption coefficient (m^{-1}), A_λ is the absorbance, and l is the optical path length of the quartz cuvette (m). The S_R value was calculated as the ratio of the spectral slope of shorter wavelengths ($S_{275-295}$) to that of longer wavelengths ($S_{350-400}$) (Helms et al., 2008; Han et al., 2020). The spectral slope (S) was calculated using the following equation:

$$a_\lambda = a_{\lambda_{ref}} e^{-S(\lambda - \lambda_{ref})} \tag{2}$$

where α is the Napierian absorption coefficient (m^{-1}), λ is the wavelength, and λ_{ref} is the reference wavelength (Twardowski et al., 2004; Helms et al., 2008).

3 Results

In 2017, the vertical distribution of salinity indicated a well-mixed water column (Fig. 2). Similarly, DO and NH_4^+ concentrations were vertically uniform (Fig. 2). Horizontally, salinity increased from 28 at the innermost station to 32 at the outermost station (Fig. 2). The concentrations of DO and NH_4^+ were in the ranges of 7–13 mg L^{-1} (average: 10.1±2.4 mg L^{-1}) and 0.1–25 μmol L^{-1} (average: 8.7±8.1 μmol L^{-1}), respectively (Fig. 2). The concentration of DO gradually increased with an increase in the salinity along the transect, while the NH_4^+ concentration decreased with an increase in the salinity (Fig. 2). The NH_4^+ concentration showed the lowest values (<1 μmol L^{-1}) between station 10 and station 13 (Fig. 2).

In 2017, the DOC concentrations were in the range of 97–349 μmol L^{-1} (average: 184±76 μmol L^{-1}). The distribution of DOC concentrations was quite different from the salinity and DO distributions, with the highest concentrations in the surface water samples of stations 3, 4, 5, 6, 7, 8, 9 and the bottom water samples of stations 3, 4, and 5 (Fig. 2). The DOC–$\delta^{13}C$ values ranged from −19.2‰ to −27.8‰ (average: −21.8±1.9‰) (Fig. 2). The most depleted values were observed in the surface water samples of stations 5, 6, 7, 9, and 10 (−22.6‰ to −27.8‰) (Fig. 2). The concentrations of $FDOM_C$ (terrestrial humic-like component 1), $FDOM_A$ (terrestrial humic-like component 2), $FDOM_M$ (marine humic-like component), and $FDOM_P$ (protein-like component) were in the ranges of 1.6–4.1 RU (average: 2.3±0.8 RU), 0.6–1.8 RU (average: 1.1±0.3 RU), 1.0–2.4 RU (average: 1.5±0.5 RU), and 1.6–6.1 RU (average: 2.8±1.0 RU), respectively (Fig. 2). The concentrations of all FDOM components were generally higher in the upstream stations and decreased with salinity (Fig. 2). The $FDOM_P$ concentration was slightly higher in the bottom water of station 10 (Fig. 2). The S_R values were in the range of 0.70–1.76 (average: 1.21±0.20), with higher values in the surface water samples of stations 6, 8, 9, and 10 (Fig. 2).

In 2018, salinity showed a wide range, between 18 and 30, compared with that in 2017 (Fig. 3). Low-salinity waters (salinity: 18–27) were observed from the innermost station to station 9 (Fig. 3). The concentrations of DO and NH_4^+ were in the ranges of 6–11 mg L^{-1} (average: 8.2±1.6 mg L^{-1}) and 0.4–25 μmol L^{-1} (average: 13.1±7.9 μmol L^{-1}), respectively (Fig. 3). The NH_4^+ concentrations in the outermost stations were lower than the detection limit (Fig. 3).

In 2018, the concentrations of DOC were in the range of 101–195 μmol L^{-1} (average: 130±32 μmol L^{-1}). The DOC concentrations gradually decreased with an increase in the salinity (Fig. 3). The DOC–$\delta^{13}C$ values ranged from −19.1‰ to −21.5‰ (average: −20.0±0.6‰) (Fig. 3). The concentrations of $FDOM_C$, $FDOM_A$, $FDOM_M$, and $FDOM_P$ were in the ranges of 1.4–5.1 RU (average: 1.9±0.9 RU), 1.3–4.1 RU (average: 1.8±0.7 RU), 1.4–4.9 RU (average: 2.1±0.9 RU), and 1.1–2.5 RU (average: 1.6±0.4 RU), respectively (Fig. 3). All $FDOM_H$ concentrations were higher in 2018 than they were in 2017 (Fig. 3). The $FDOM_P$ concentrations were generally higher in the surface water samples, with a slightly higher value at station 12, where the salinity is slightly lower (Fig. 3). The S_R values were in the range of 0.72–1.08 (average: 0.87±0.10) (Fig. 3). The S_R values were relatively constant at all sampling stations (Fig. 3).

4 Discussion

In both sampling periods, low-salinity waters showed higher DOC, lower DO, higher NH_4^+, and higher $FDOM_H$ ($FDOM_C$) concentrations (Figs. 2 and 3). As such, the DOC and $FDOM_H$ concentrations exhibited significant negative correlations against salinity, indicating low-salinity-associated inputs of both DOM components (Figs. 4a and 4b). However, the patterns of the DOC distributions were very different from those of the $FDOM_H$ distributions, indicating the decoupling of the major sources for both DOM components (Figs. 2 and 3). In this region, anthropogenic source inputs were found to be insignificant since there were no anomalous increases in DOC and $FDOM_H$ concentrations in 2018 at station B4, where the waterway connects to the Banwol industrial complex (Fig. 3).

In both periods, the concentrations of $FDOM_H$ showed significant correlations against salinities and NH_4^+ concentrations, with two negative slopes against salinity and a single positive slope against NH_4^+ (Figs. 4 and 5). This correlation trend suggests that the main source of $FDOM_H$ was dependent on the supply of NH_4^+, rather than freshwater inputs (Figs. 4a and 5a). In this lake, Kim and Kim (2018) hypothesized that $FDOM_H$ is produced by the anaerobic decomposition of organic matter in bottom sediments in the freshwater-seawater mixing zone, based on good correlations among the salinity, NH_4^+, and $FDOM_H$ concentrations as well as low Eh values in samples with higher $FDOM_H$ concentrations, although possible terrestrial inputs could not be excluded. Such correlations could also be observed if terrestrial fresh water, which has higher $FDOM_H$ and lower NH_4^+ levels, passes through a salinity mixing zone where extremely high amounts of NH_4^+ and low $FDOM_H$ are introduced from bottom sediments. However, our DOC–$\delta^{13}C$ values ($-20.0\pm0.4‰$) observed in low-salinity (<28) water samples here exclude any possible significant contributions of terrestrial sources, indicating the effective degradation of terrestrial sources before they reached the mixing zone. In this tidal flat environment, the large inputs (i.e., seepage) of DOC and $FDOM_H$, together with NH_4^+, may have happened from marine sediments without significant decreases in the DO concentration (Kim et al., 2012), as the shore water runs back and forth over a wide sediment-surface area during tidal cycles (Fig. 5). In this case, depending on the salinity ranges of the overlying waters, different slopes of $FDOM_H$ against salinities could be observed for different seasons as observed in this study (Fig. 4b).

In 2018, the distribution pattern of the DOC concentrations was similar to that of $FDOM_H$ (Fig. 3). During this period, the freshwater contribution was greater compared with that in 2017, with the lowest salinity being approximately 18. However, the DOC–$\delta^{13}C$ values in all samples in this period ranged from $-19.1‰$ to $-21.5‰$ (average: $-20.0\pm0.6‰$), falling into the range of marine phytoplankton values ($-18‰$ to $-22‰$) (Gearing, 1988) (Fig. 4c). The S_R values were relatively low and constant (average: 0.86 ± 0.1) at all stations in 2018, indicating no significant changes in the input sources or the effects of photochemical and bacterial degradation (Moran et al., 2000; Helms et al., 2008) (Fig. 4d). Thus, we conclude that the main source of DOC in 2018 was from marine sediments, together with $FDOM_H$ and NH_4, as external terrestrial sources of DOC were insignificant or effectively degraded on the tidal flat (Kim et al., 2012).

In 2017, the sources of DOC were more complicated, showing large excess DOC concentrations independent of salinity (Fig. 2). Here, this excess denotes concentrations higher than that of the incoming seawater (background) from the Yellow Sea (highest salinity and lowest DOC concentrations) observed in 2018 (Fig. 4a). The samples with excess DOC levels observed in 2017 were nearly 69% higher than the DOC values of the background seawater (~110 µmol L^{-1}) (Fig. 4a). The samples with higher DOC levels observed in 2017 were separated into two major groups (Group 1 and Group 2) based on their DOC concentrations, DOC–δ^{13}C values, and salinities (Fig. 2). Group 1 (*n=3*) includes the samples observed in stations 12 and 13 (Fig. 2). Group 2 (*n=11*) includes the samples observed in the surface waters of stations 4, 5, 6, 7, 8, 9, and 10, and in the bottom waters of stations 3, 4, 5, and 6 (Fig. 2).

For the Group 1 samples, the DOC concentrations ranged from 144 to 223 µmol L^{-1} (average: 175±42 µmol L^{-1}) (Figs. 2 and 4a). The DOC–δ^{13}C values ranged from –19.1‰ to –22.1‰ (average: –20.6±1.5‰), which are close to the δ^{13}C values of marine organisms (Figs. 2 and 4c). The S_R values (average: 1.07±0.03) in this group were relatively low and constant compared with that of Group 2 (Figs. 2 and 4d). Thus, the higher DOC concentrations observed in this group appear to be from in-situ biological production.

For the Group 2 samples, the DOC concentrations ranged from 103 to 330 µmol L^{-1} (average: 213±69 µmol L^{-1}) (Figs. 2 and 4a). The DOC–δ^{13}C values ranged from –21.5‰ to –27.8‰, which include the signature of terrestrial C$_3$ plants (–23‰ to –32‰) (Gearing, 1988) (Figs. 2 and 4c). For this group, increases in FDOM$_H$ concentrations were not observed, although the S_R values (average: 1.26±0.2) were higher than those at other stations, likely due to the influence of highly degraded low-molecular-weight DOM (Helms et al., 2008) (Fig. 4d). Thus, this terrestrial DOM observed in 2017 seems to be associated with non-fluorescent and low-molecular-weight DOM on the reclaimed land by direct land-seawater interaction through the tidal inundation of seawater. This could happen if the terrestrial DOM experienced intense light exposure and/or bacterial degradation on land, a condition likely facilitated through the process of land reclamation.

Without the use of these multiple tracers, in this region, the higher DOC and FDOM$_H$ concentrations occurring in areas with lower salinity waters could be attributed to inputs with terrestrial origins, while the higher DOC concentrations in high salinity areas could be attributed to in-situ biological production. However, these multiple tracers can lead to the better identification of different source inputs. Therefore, our results suggest that the combination of stable carbon isotope, FDOM, and S_R values can be a critical tool for deciphering the sources and characteristics of DOM in coastal waters where various DOM sources are present.

5 Conclusions

Different sources and distributions of DOM were determined in different seasons using various tracers in Sihwa Lake, South
225 Korea. Our results reveal that the higher DOC concentrations occurring in low-salinity water, which could be regarded as having terrestrial sources, were actually from marine sediment sources based on DOC–δ^{13}C values (–19.1‰ to –21.5‰) together with significant correlations among the DOC, $FDOM_H$, and NH_4^+ concentrations. On the other hand, the excess DOC concentrations occurring in high-salinity waters at some stations, which are generally believed to be from marine sources, were found to be from non-fluorescent, low-molecular-weight, terrestrial DOM sources from the reclaimed land
230 area based on depleted DOC–δ^{13}C values (–21.5‰ to –27.8‰) and high S_R values (1.26±0.2), without concurrent increases in the $FDOM_H$ and NH_4^+ concentrations. Our study demonstrates that the combination of these multiple DOM tracers can be used successfully in other coastal waters where the sources and characteristics of DOM are complicated.

Data availability. All data are available upon request to the corresponding author.
235

Author contributions. GK contributed to the conceptualization of the manuscript. HH and GK were involved in planning the research. HH collected samples and performed the analyses. All authors were involved in analyzing the results and writing the paper.

240 *Competing interests.* The authors declare that they have no conflict of interest.

Acknowledgements. This research was supported by the National Research Foundation (NRF) of Korea (NRF-2018R1A2B3001147) funded by the South Korean government. We would like to thank all lab members for their assistance.

References

245 Bae, Y. H., Kim, K. O., and Choi, B. H.: Lake Sihwa tidal power plant project, Ocean. Eng., 37, 454–463, https://doi.org/10.1016/j.oceaneng.2010.01.015, 2010.

Bauer, J. E. and Bianchi, T. S.: Dissolved organic carbon cycling and transformation, in: Treatise on estuarine and coastal science, edited by: Wolanski, E. and Mcluski, D. S., 5, 7–67, Academic Press, Waltham, 2011.

Benner, R., Pakulski, J. D., McCarthy, M., Hedges, J. I., and Hatcher, P. G.: Bulk chemical characteristics of dissolved
250 organic matter in the ocean, Science, 255, 1561–1564, https://doi.org/10.1126/science.255.5051.1561, 1992.

Bro, R.: PARAFAC. Tutorial and applications, Chemometr. Intell. Lab., 38, 149–171, 1997.

Carlson, C. A. and Hansell, D. A.: Chapter 3 – DOM sources, sinks, reactivity, and budgets, in: Biogeochemistry of marine dissolved organic matter (Second Edition), edited by: Hansell, D. A. and Carlson, C. A., 65–126, Academic Press, Boston, 2015.

255   Carpenter, J. H.: The Chesapeake Bay institute technique for the Winkler dissolved oxygen method, Limnol. Oceanogr., 10, 141–143, 1965.

Catalá, T. S., Reche, I., Álvarez, M., Khatiwala, S., Guallart, E. F., Benítez-Barrios, V. M., Fuentes-Lema, A., Romera-Castillo, C., Nieto-Cid, M., Pelejero, C., Fraile-Nuez, E., Ortega-Retuerta, E., Marrasé, C., and Álvarez-Salgado, X. A.: Water mass age and aging driving chromophoric dissolved organic matter in the dark global ocean, Global

260   Biogeochem. Cy., 29, 917–934, https://doi.org/10.1002/2014GB005048, 2015.

Coble, P. G.: Characterization of marine and terrestrial DOM in seawater using excitation-emission matrix spectroscopy, Mar. Chem., 51, 325–346, https://doi.org/10.1016/0304-4203(95)00062-3, 1996.

Coble, P. G.: Marine optical biogeochemistry: the chemistry of ocean color, Chem. Rev., 107, 402–418, https://doi.org/10.1021/cr050350+, 2007.

265   Gearing, J. N.: The use of stable isotope ratios of tracing the nearshore-offshore exchange of organic matter, in: Coastal-offshore ecosystem interactions, edited by: Jansson, B.-O., 69–101, Springer-Verlag, Berlin, 1988.

Griffith, D. R. and Raymond, P. A.: Multiple-source heterotrophy fuelled by aged organic carbon in an urbanized estuary, Mar. Chem., 124, 14–22, https://doi.org/10.1016/j.marchem.2010.11.003, 2011.

Han, H., Kim, G., Seo, H., Shin, K.-H., and Lee, D.-H.: Significant seasonal changes in optical properties of brown carbon in

270   the midlatitude atmosphere, Atmos. Chem. Phys., 20, 2709–2718, https://doi.org/10.5194/acp-20-2709-2020, 2020.

Hansell, D. A.: Dissolved organic carbon reference material program, Eos Trans. AGU., 86, 318, https://doi.org/10.1029/2005EO350003, 2005.

Hansen, A. M., Kraus, T. E. C., Pellerin, B. A., Fleck, J. A., Downing, B. D., and Bergamaschi, B. A.: Optical properties of dissolved organic matter (DOM): Effects of biological and photolytic degradation, Limnol. Oceanogr., 61, 1015–1032,

275   https://doi.org/10.1002/lno.10270, 2016.

Helms, J. R., Stubbins, A., Ritchie, J. D., and Minor, E. C.: Absorption spectral slopes and slope ratios as indicators of molecular weight, source, and photobleaching of chromophoric dissolved organic matter, Limnol. Oceanogr., 53, 955–969, https://doi.org/10.4319/lo.2008.53.3.0955, 2008.

Jørgensen, L., Stedmon, C. A., Kragh, T., Markager, S., Middelboe, M., Søndergaard, M.: Global trends in the fluorescence

280   characteristics and distribution of marine dissolved organic matter, Mar. Chem., 126, 139–148, https://doi.org/10.1016/j.marchem.2011.05.002, 2011.

Kim, J. and Kim, G.: Significant anaerobic production of fluorescent dissolved organic matter in the deep East Sea (Sea of Japan), Geophys. Res. Lett., 43, 7609–7616, https://doi.org/10.1002/2016GL069335, 2016.

Kim, J. and Kim, T.-H.: Distribution of humic fluorescent dissolved organic matter in lake Shihwa: the role of the redox

285   condition, Estuar. Coast., https://doi.org/10.1007/s12237-018-00491-0, 2018.

Kim, K. T., Kim, E. S., Cho, S. R., and Park, J. K.: Distribution and temporal change of heavy metals in the surface sediments of lake Shihwa and adjacent sea, Korea, J. Coast. Res., 56, 817–821, 2009.

Kim, T.-H. and Kim, G.: Distribution of dissolved organic carbon (DOC) in the southwestern East Sea in summer, Ocean Polar Res., 32, 291–297, 2010.

290   Kim, T.-H. and Kim, G.: Estimating benthic fluxes of trace elements to hypoxic coastal waters using [210]Po, Estuar. Coast. Shelf. Sci., 151, 324–330, https://doi.org/10.1016/j.ecss.2014.05.008, 2014.

Kim, T.-H., Waska, H., Kwon, E., Suryaputra, G. N., and Kim, G.: Production, degradation, and flux of dissolved organic matter in the subterranean estuary of a large tidal flat, Mar. Chem., 142–144, 1–10, http://dx.doi.org/10.1016/j.marchem.2012.08.002, 2012.

295   Koepfler, E. T., Benner, R., and Montagna, P. A.: Variability of dissolved organic carbon in sediments of a Seagrass bed and an unvegetated area within an estuary in Southern Texas, Estuaries, 16, 391–404, 1993.

Lang, S. Q., Lilley, M. D., and Hedge, J. I.: A method to measure the isotopic (^{13}C) composition of dissolved organic carbon using a high temperature combustion instrument, Mar. Chem., 103, 318–326, 2007.

Lawaetz, A. J. and Stedmon, C. A.: Fluorescence intensity calibration using the raman scatter peak of water, Appl.
300   Spectrosc., 62, 936–940, 2009.

Lee, C.-H., Lee, B.-Y., Chang, W. K., Hong, S., Song, S. J., Park, J., Kwon, B., Khim, J. S.: Environmental and ecological effects of Lake Shihwa reclamation project in South Korea: A review, Ocean. Coast. Manage., 102, 545–558, https://doi.org/10.1016/j.ocecoaman.2013.12.018, 2014.

Lee, J., Hong, S., Yoon, S. J., Kwon, B., Ryu, J., Giesy, J. P., Allam, A. A., Al-khedhairy, A. A., and Khim, J. S.: Long-term
305   changes in distributions of dioxin-like and estrogenic compounds in sediments of Lake Sihwa, Korea: Revisited mass balance, Chemosphere, 181, 767–777, https://doi.org/10.1016/j.chemosphere.2017.04.074, 2017.

Lee, S.-A., Kim, T.-H., and Kim, G.: Tracing terrestrial versus marine sources of dissolved organic carbon in a coastal bay using stable carbon isotopes, Biogeosciences, 17, 135–144, https://doi.org/10.5194/bg-17-135-2020, 2020.

Lee, S.-I., Kim, B.-C., and Oh, H.-J.: Evaluation of lake modification alternatives for Lake Sihwa, Korea, Environ. Manage.,
310   29, 57–66, https://doi.org/10.1007/s00267-001-0040-0, 2002.

Moran, M. A., Sheldon, W. M., and Zepp, R. G.: Carbon loss and optical property changes during long-term photochemical and biological degradation of estuarine dissolved organic matter, Limnol. Oceanogr., 45, 1254–1264, 2000.

Murphy, K. R., Stedmon, C. A., Wenig, P., and Bro, R.: OpenFluor- an online spectral library of auto-fluorescence by organic compounds in the environment, Anal. Methods., 6, 658–661, https://doi.org/10.1039/C3AY41935E, 2014.

315   Opsahl, S. and Benner, R.: Distribution and cycling of terrigenous dissolved organic matter in the ocean, Nature, 386, 480–482, https://doi.org/10.1038/386480a0, 1997.

Panetta, R. J., Ibrahim, M., and Gélinas, Y.: Coupling a high-temperature catalytic oxidation total organic carbon analyzer to an isotope ratio mass spectrometer to measure natural-abundance δ^{13}C-dissolved organic carbon in marine and freshwater samples, Anal. Chem., 80, 5232–5239, https://doi.org/10.1021/ac702641z, 2008.

320   Ra, K., Bang, J.-H., Lee, J.-M., Kim, K.-T., and Kim, E.-S.: The extent and historical trend of metal pollution recorded in core sediments from the artificial Lake Shihwa, Korea, Mar. Pollut. Bull., 62, 1814–1821, https://doi.org/10.1016/j.marpolbul.2011.05.010, 2011.

Raymond, P. A. and Spencer, R. G. M.: Chapter 11 – Riverine DOM, in: Biogeochemistry of marine dissolved organic matter (Second Edition), edited by: Hansell, D. A. and Carlson, C. A., 509–535, Academic Press, Boston, 2015.

325   Stedmon, C. A. and Bro, R.: Characterizing dissolved organic matter fluorescence with parallel factor analysis: a tutorial, Limnol. Oceanogr-Meth.,6, 572–579, 2008.

Stedmon, C. A. and Nelson, N. B.: Chapter 10 – The optical properties of DOM in the ocean, in: Biogeochemistry of marine dissolved organic matter (Second Edition), edited by: Hansell, D. A. and Carlson, C. A., 481–508, Academic Press, Boston, 2015.

330   Tedetti, M., Guigue, C., and Goutx, M.: Utilization of a submersible UV fluorometer for monitoring anthropogenic inputs in the Mediterranean coastal waters, Mar. Pollut. Bull., 60, 350–362, https://doi.org/10.1016/j.marpolbul.2009.10.018, 2010.

Troyer, I. D., Bouillon, S., Barker, S., Perry, C., Coorevits, K., and Merckx, R.: Stable isotope analysis of dissolved organic carbon in soil solutions using a catalytic combustion total organic carbon analyzer-isotope ratio mass spectrometer with
335   a cryofocusing interface, Rapid Commun. Mass Spectrom., 24, 365–374, https://doi.org/10.1002/rcm.4403, 2010.

Twardowski, M. S., Boss, E., Sullivan, J. M., and Donaghay, P. L.: Modeling the spectral shape of absorbing chromophoric dissolved organic matter, Mar. Chem., 89, 69–88, https://doi.org/10.1016/j.marchem.2004.02.008, 2004.

Vetter, T. A., Perdue, E. M., Ingall, E., Koprivnjak, J.-F., and Pfromm, P. H.: Combining reverse osmosis and electrodialysis for more complete recovery of dissolved organic matter from seawater, Sep. Purif. Technol., 56, 383–387,
340   https://doi.org/10.1016/j.seppur.2007.04.012, 2007.

Wang, X.-C., Chen, R. F., and Gardner, G. B.: Sources and transport of dissolved and particulate organic carbon in the Mississippi River estuary and adjacent coastal waters of the northern Gulf of Mexico, Mar. Chem., 89, 241–256, https://doi.org/10.1016/j.marchem.2004.02.014, 2004.

Zepp, R. G., Sheldon, W. M., and Moran, M. A.: Dissolved organic fluorophores in southeastern US coastal waters:
345   correction method for eliminating Rayleigh and Raman scattering peaks in excitation-emission matrices, Mar. Chem., 89, 15–36, https://doi.org/10.1016/j.marchem.2004.02.006, 2004.

350

355

360
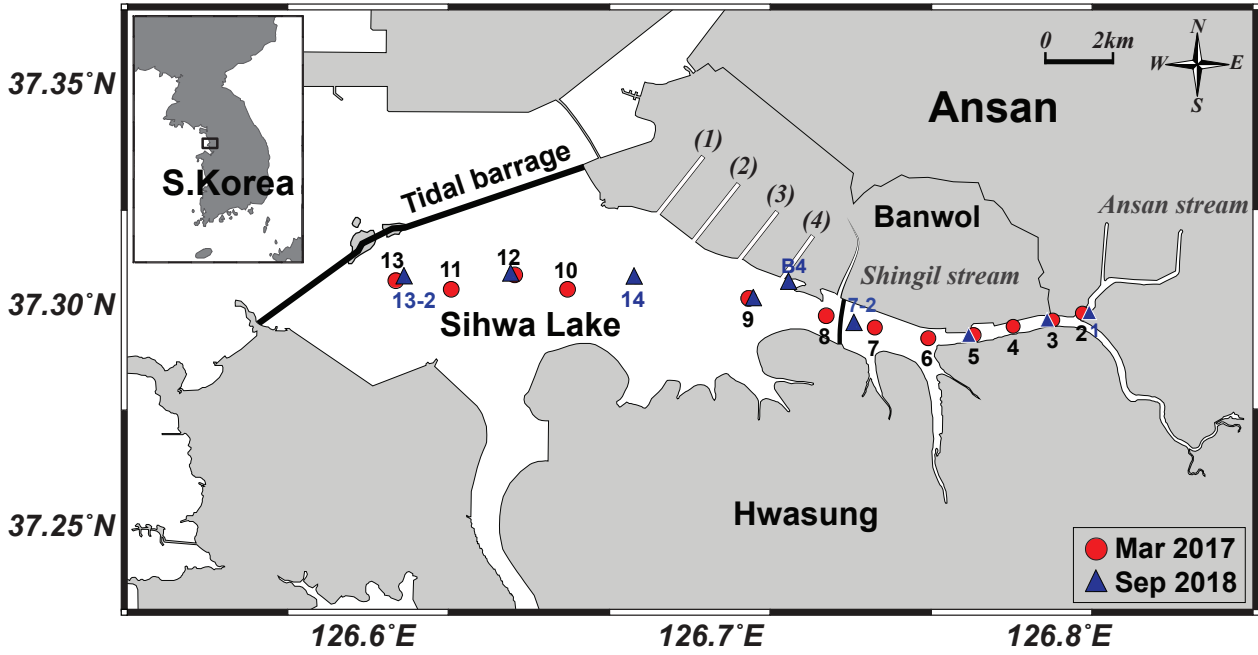
Figure 1: Map of sampling stations in Sihwa Lake, South Korea.

365
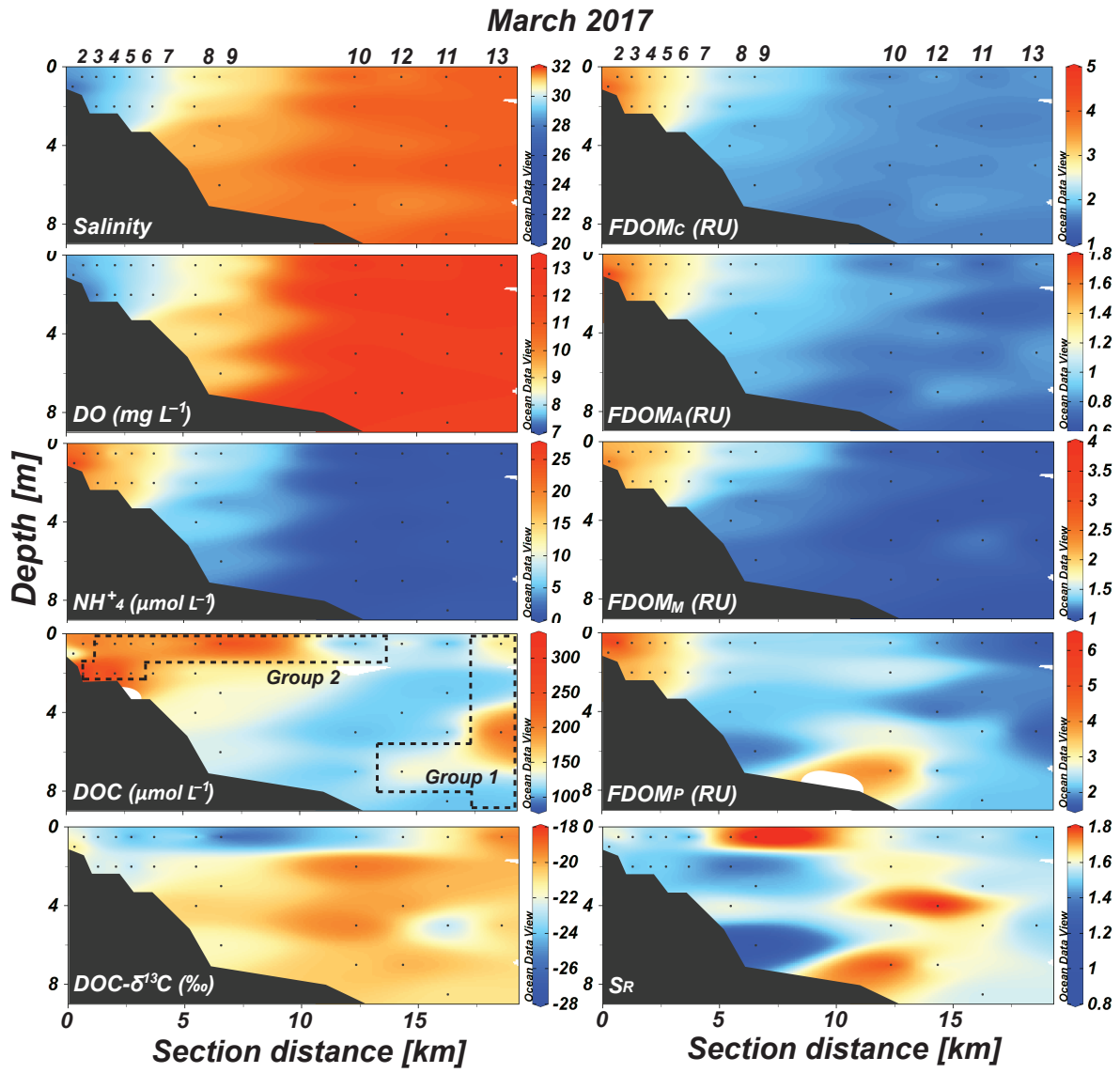
Figure 2: Vertical distributions of salinity, DO, NH₄⁺, DOC, DOC–δ¹³C, FDOM_C, FDOM_A, FDOM_M, FDOM_P, and S_R values in Sihwa Lake in March 2017. The dashed blocks represent stations belonging to the Group 1 and the Group 2, which were separated based on the distributions of DOC, DOC–δ¹³C, and salinity.

370
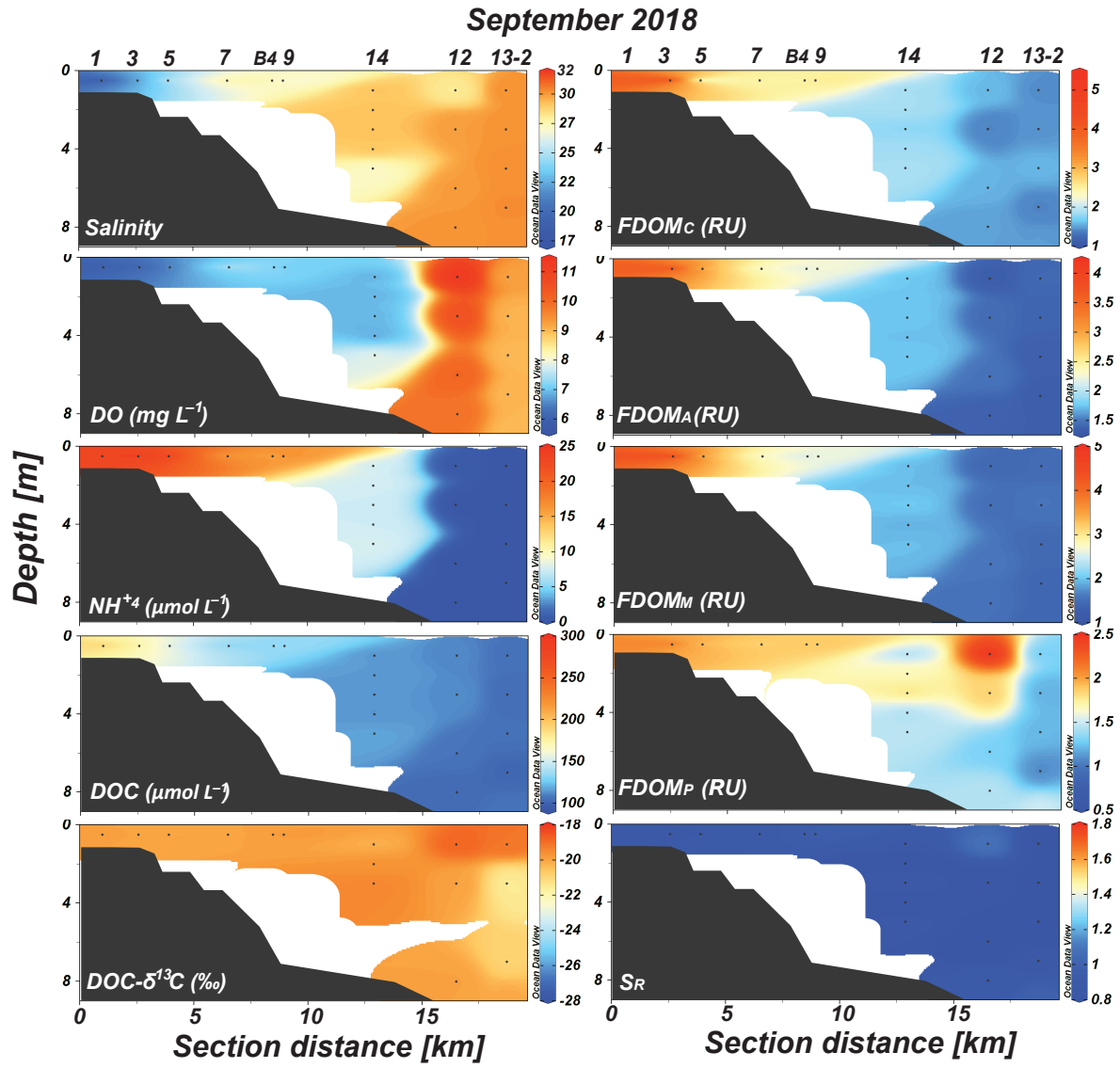
Figure 3: Vertical distributions of salinity, DO, NH$_4^+$, DOC, DOC–δ^{13}C, FDOM$_C$, FDOM$_A$, FDOM$_M$, FDOM$_P$, and S_R values in Sihwa Lake in September 2018.
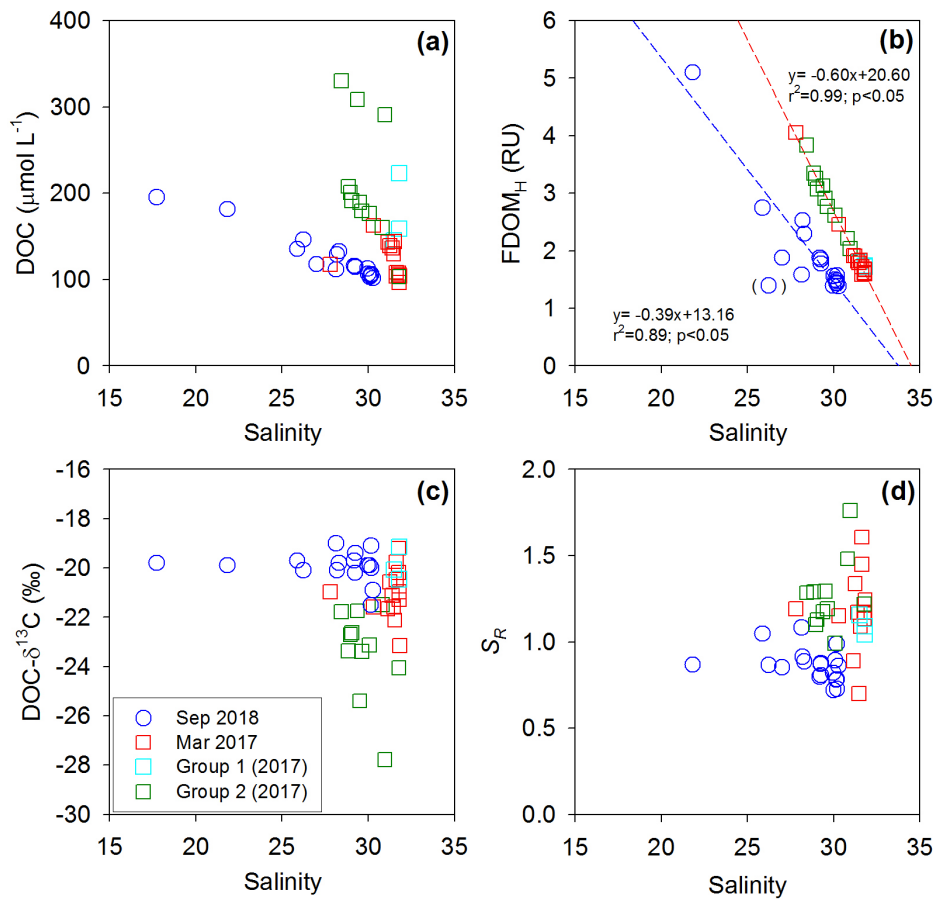
385

Figure 4: Plots of salinity versus (a) DOC concentrations, (b) FDOM$_H$ concentrations, (c) DOC–δ^{13}C values, and (d) S_R values in Sihwa Lake in March 2017 (red square) and September 2018 (blue circle). The dashed lines represent the regression lines.
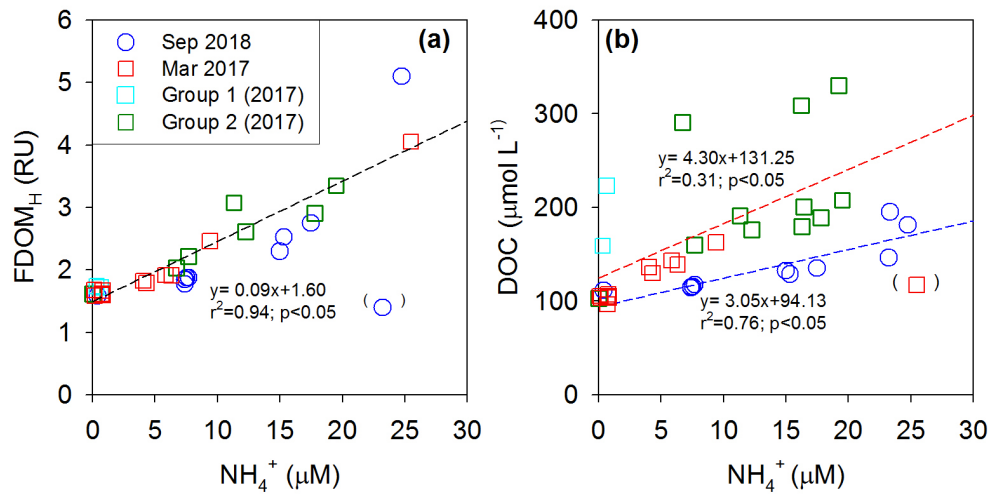
390

Figure 5: Plots of NH$_4^+$ concentrations versus (a) FDOM$_H$ concentrations and (b) DOC concentrations in Sihwa Lake in March 2017 (red square) and September 2018 (blue circle). The dashed lines represent the regression lines.